Systemic Brain Delivery of Antisense Oligonucleotides across the Blood–Brain Barrier with a Glucose-Coated Polymeric Nanocarrier

Hyun Su Min[+], Hyun Jin Kim[+], Mitsuru Naito, Satomi Ogura, Kazuko Toh, Kotaro Hayashi, Beob Soo Kim, Shigeto Fukushima, Yasutaka Anraku, Kanjiro Miyata,* and Kazunori Kataoka*

Abstract: *Current antisense oligonucleotide (ASO) therapies for the treatment of central nervous system (CNS) disorders are performed through invasive administration, thereby placing a major burden on patients. To alleviate this burden, we herein report systemic ASO delivery to the brain by crossing the blood–brain barrier using glycemic control as an external trigger. Glucose-coated polymeric nanocarriers, which can be bound by glucose transporter-1 expressed on the brain capillary endothelial cells, are designed for stable encapsulation of ASOs, with a particle size of about 45 nm and an adequate glucose-ligand density. The optimized nanocarrier efficiently accumulates in the brain tissue 1 h after intravenous administration and exhibits significant knockdown of a target long non-coding RNA in various brain regions, including the cerebral cortex and hippocampus. These results demonstrate that the glucose-modified polymeric nanocarriers enable non-invasive ASO administration to the brain for the treatment of CNS disorders.*

Introduction

Recently, antisense oligonucleotide (ASO) therapies have been rigorously developed for the treatment of central nervous system (CNS) disorders, such as Alzheimer's disease, Huntington's disease (HD), and amyotrophic lateral sclerosis (ALS).[1,2] This development relies on the fact that ASOs can delay the disease onset or halt the disease progression through target gene knockdown or splicing modulation.[3] In 2018, Spinraza® was approved as an ASO drug (or a splicing modulator for the survival motor neuron gene) for the treatment of spinal muscular atrophy by the US Food and Drug Administration.[4] However, such ASO drugs require administration by highly invasive routes, for example, intrathecal or intracerebroventricular administration, because the accessibility (or availability) of ASO drugs to the CNS through the bloodstream is miserably low due to the tightly connected cerebrovascular endothelium or brain capillary endothelial cells (BCECs), that is, the blood–brain barrier (BBB).[5] The BBB prevents free permeation of molecules larger than 400 Da, including ASO drugs (approximately 7000 Da), between the bloodstream and the brain parenchyma.[5] Therefore, systemic ASO delivery to the brain remains to be one of the most challenging issues in drug delivery and ASO therapeutics.[1] Here, with the aim of tackling this issue, we developed multiple glucose-modified nanocarriers capable of crossing the BBB with the aid of active translocation of glucose-transporter 1 (GLUT1) from the apical to the basal side of the BCECs.

A major reason to focus on GLUT1, a protein of 54 kDa that is abundantly expressed on the plasma membrane surface of the BCECs,[6] is its unique feature that has been recently discovered by our group:[7] it undergoes prompt translocation from the apical to the basal side of the BCEC membrane, presumably through the *endo-/exo*-cytosis (transcytosis) process, responding to an increase in blood glucose level after 16–24 h of fasting (glycemic control). Interestingly, systemically injected glucose-modified nanoparticles that exhibit multivalent interaction with GLUT1 molecules on the apical side of the BCECs are carried together with the GLUT1 molecules toward the basal side of the BCECs under the condition of glycemic control, and are ultimately released into the brain parenchyma. Apparently, the binding/dissociation

[*] Dr. H. S. Min,[+] S. Ogura, Dr. B. S. Kim, Prof. K. Miyata
Department of Materials Engineering,
Graduate School of Engineering, The University of Tokyo
7-3-1 Hongo, Bunkyo-ku, Tokyo 113-8656 (Japan)
E-mail: miyata@bmw.t.u-tokyo.ac.jp

Dr. H. J. Kim,[+] Dr. M. Naito
Center for Disease Biology and Integrative Medicine,
Graduate School of Medicine, The University of Tokyo
7-3-1 Hongo, Bunkyo-ku, Tokyo 113-0033 (Japan)

Dr. K. Toh, Dr. K. Hayashi, S. Fukushima, Dr. Y. Anraku,
Prof. K. Kataoka
Innovation Center of Nanomedicine (iCONM),
Kawasaki Institute of Industrial Promotion
3-25-14 Tonomachi, Kawasaki-ku, Kawasaki 210-0821 (Japan)
E-mail: kataoka@ifi.u-tokyo.ac.jp

Dr. Y. Anraku
Department of Bioengineering, Graduate School of Engineering,
The University of Tokyo
7-3-1 Hongo, Bunkyo-ku, Tokyo 113-8656 (Japan)

Prof. K. Kataoka
Institute for Future Initiatives, The University of Tokyo
7-3-1 Hongo, Bunkyo-ku, Tokyo 113-0033 (Japan)

[+] These authors contributed equally to this work.

Supporting information and the ORCID identification number(s) for the author(s) of this article can be found under:
https://doi.org/10.1002/anie.201914751.

balance of glucose-modified nanoparticles to/from GLUT1 molecules is important in this serial process of binding–translocation–releasing; the appreciably low affinity of glucose to GLUT1 ($K_D = 3$ mM)[8] is favorable because the binding/dissociation balance can be managed over a wide range by varying the number and density of glucose ligands on each of the nanoparticles. This regulates the multivalent interactions, by which the whole affinity is determined as the integration of the weak affinity between each of the components,[9] in this case GLUT1 and glucose.

The key characteristics required for the development of a BBB-crossing nanocarrier for ASO delivery are the following: 1) longevity in the blood circulation after systemic injection, 2) feasible density tuning of the glucose ligands exposed on the nanocarrier surface to optimize GLUT1-mediated transport across the BCEC layer, and 3) smooth cargo ASO release in the appropriate site of action in the brain parenchyma. Thus, we chose a polyion complex micelle (PIC/M) self-assembled from poly(ethylene glycol)-*b*-poly(L-lysine) modified with 3-mercaptopropyl amidine and 2-thiolaneimine (PEG-PLL(MPA/IM)) block copolymer and ASO through electrostatic interaction as the platform structure for the BBB-crossing nanocarrier.[10–12] The ASO in PIC/M is captured in the core, surrounded by the shell of densely associated PEG strands to ensure longevity in blood circulation. Furthermore, disulfide crosslinking is introduced in the PIC/M core by partially derivatizing the side chain of the poly(L-lysine) segment in the PEG-PLL with sulfhydryl groups (Figure 1).[10–12] In this way, while the PIC/M becomes more robust in the nonreductive blood compartment due to the formation of disulfide crosslinking in the core, it undergoes destabilization in the reductive condition of the brain through the cleavage of disulfide bonds to release the cargo ASO. The 2-thiolaneimine groups are also introduced in the poly(L-lysine) segment to further stabilize the micelle structure through hydrophobic/dipole interactions. It is worthy emphasizing that density tuning of the glucose-ligands on the PIC/M surface is easily achieved by changing the mixing ratio of the block copolymers with and without the glucose moiety at the distal end of the PEG segment.
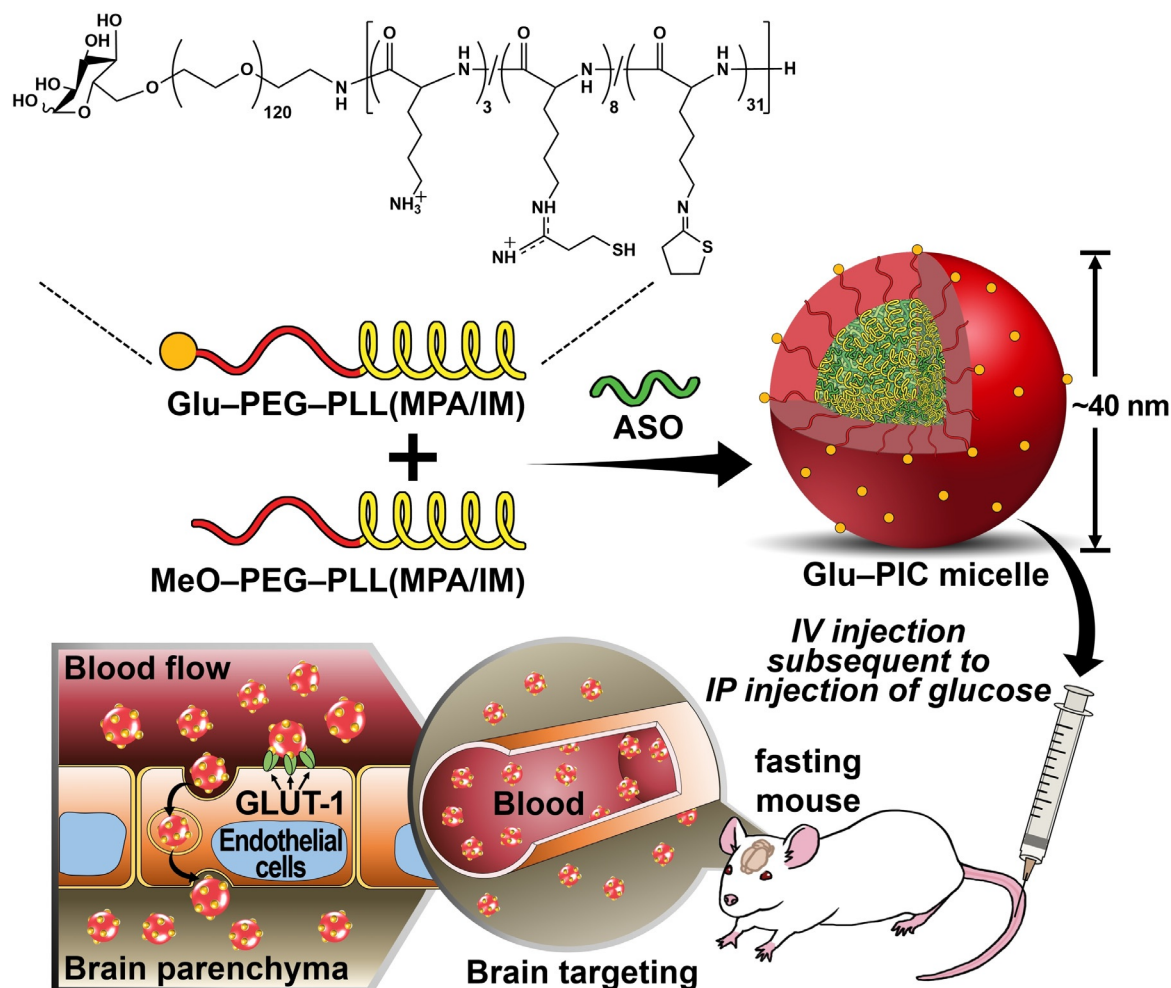

Figure 1. Schematic illustration of the present study for systemic ASO delivery to the brain. ASO-loaded glucosylated-polyion complex micelles (Glu-PIC/Ms) are prepared from the ASO and a mixture of Glu-PEG-PLL(MPA/IM) and MeO-PEG-PLL(MPA/IM) with varying numbers of glucose ligands on the PIC/Ms. The glucose solution is intraperitoneally injected into overnight-fasting mice to trigger GLUT1 translocation and recycling. Then, Glu-PIC/Ms are intravenously administrated into the mice for the GLUT1-mediated transcytosis from the bloodstream to the brain parenchyma.

As described above, ASO-loaded glucosyl-PIC/M with optimized composition was prepared, aiming to achieve delivery of ASO into multiple regions of the brain parenchyma with appreciably high efficiency (approximately 6% dose g^{-1} of brain) within 1 h after intravenous administration under glycemic control. Furthermore, knockdown of the model target non-coding RNA, the metastasis-associated lung adenocarcinoma transcript 1 (*MALAT1*) long non-coding RNA (lncRNA), as high as 40%, was achieved in the major regions of the brain, namely, the cerebral cortex and hippocampus; this was achieved by just a single intravenous injection, indicating a promising utility of ASO-loaded glucosyl-PIC/M for the treatment of various CNS disorders using the systemic route.

Results and Discussion

Preparation and Characterization of the Glu-PIC/Ms

For the synthesis of Glu-PEG-PLL(MPA/IM), a hetero bifunctional PEG with 1,2:3,5-di-*O*-isopropylidene-α-D-glucofuranose at the α-end, and primary amine at the ω-end (DIG-PEG-NH$_2$), with a molecular weight of the PEG (MW$_{PEG}$) of 5300 Da, was synthesized by living anionic polymerization of ethylene oxide initiated with a potassium alkolate of DIG, as previously described (Supporting Information, Figure S1).[13] The PEG segment was extended from the hydroxyl group at the C6 position of DIG to generate hydroxyl groups at the C1, C3, and C4 positions after deprotection of DIG. It is important to note that these three hydroxyl groups in the glucose moiety are critical for successful binding to GLUT1.[14] DIG-PEG-PLL(TFA) was then synthesized by the ring-opening polymerization of ε-trifluoroacethyl-L-lysine *N*-carboxy anhydride (Lys(TFA)-NCA) with DIG-PEG-NH$_2$ as a macroinitiator. Glu-PEG-PLL was obtained after deprotection of the TFA and isopropylidene acetal moieties. The degree of polymerization (DP) of the PLL segment (DP$_{PLL}$) was determined to be 42 from the ^{1}H NMR spectrum, and the molecular weight

distribution was confirmed to be unimodal by size exclusion chromatography (Supporting Information, Figure S2). Glu-PEG-PLL was reacted with two different sulfide linkers, dimethyl 3,3′-dithiobispropionimidate/2HCl and 2-iminothiolane/HCl, in the PLL side chains to obtain Glu-PEG-PLL-(MPA/IM) (Supporting Information, Figure S1). The obtained polymer was determined to possess 8 MPA and 31 IM moieties in the PLL side chains from the ^{1}H NMR spectrum (Supporting Information, Figure S3). MeO-PEG-PLL(MPA/IM) (MW$_{PEG}$: 5000 Da; DP$_{PLL}$: 42) was similarly synthesized as a non-targeted control polymer and characterized to contain 6 MPA and 35 IM moieties (Supporting Information, Figure S4).

PIC formation between the block copolymer and the ASO was first investigated using MeO-PEG-PLL(MPA/IM) (MeO-polymer) in the buffer with varying concentrations of NaCl to manipulate the micelle size. It is noteworthy that the *MALAT1* ASO used in this study was a locked nucleic acid (LNA)-modified gapmer structure with a phosphorothioate linkage backbone because it strongly tolerates enzymatic degradation and exhibits a high affinity to the target lncRNA for efficient gene-silencing activity.[15] The block copolymer was dissolved in 10 mM HEPES buffer (pH 7.3) with varying concentrations of NaCl and then mixed with the ASO dissolved in the same buffer in the absence of NaCl. The mixed solutions were dialyzed against the 10 mM HEPES buffer (pH 7.3) in the absence of NaCl for 3 days, followed by dynamic light scattering measurement (Figure 2 A). The PIC sample prepared at 0 mM NaCl exhibited a size of approximately 80 nm and a polydispersity index (PDI) of approximately 0.2. An increase in NaCl concentration gradually reduced the size and PDI of the PIC samples. At 100 mM NaCl, the size of the PIC sample was approximately 40 nm with a PDI of approximately 0.1.

The stability of the PIC/Ms under dilute conditions was further examined by fluorescence correlation spectroscopy (FCS), which is suitable for size measurement under highly dilute conditions.[16,17] PIC samples were prepared from MeO-polymer and Alexa-Fluor-647-labeled ASO (A647-ASO) at 5 μM ASO concentration with or without 100 mM NaCl. Then,
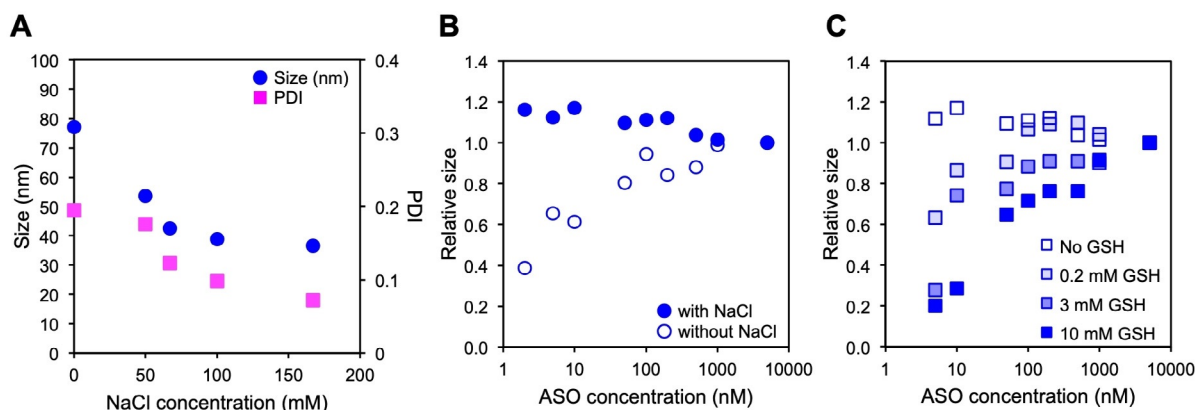

Figure 2. Characterization of ASO-loaded PIC/Ms prepared from MeO-polymer. A) Sizes and PDIs of PIC/Ms prepared at various NaCl concentrations, determined by dynamic light scattering. B) Change in the relative size of A647-ASO-loaded PIC/Ms prepared at 0 or 100 mM NaCl, determined by FCS. C) Change in the relative size of A647-ASO-loaded PIC/Ms prepared at 100 mM NaCl after treatment with/without GSH, determined by FCS. A647-ASO-loaded PIC/Ms were diluted at designated ASO concentrations and incubated with GSH for 1 h at 37°C.

the sizes of the PIC/Ms were determined at serially diluted ASO concentrations (Figure 2B). The sizes of the PIC/Ms prepared at 100 mM NaCl were maintained even after 1000-fold volume dilution. In contrast, the sizes of the PIC/Ms prepared without NaCl progressively decreased, indicating the dissociation of the PICs. These results demonstrated that NaCl treatment enhanced PIC stability. The free thiol contents in PIC/Ms determined by Ellman's assay were almost similar between 0 and 100 mM NaCl (approximately 85% of thiols were converted to disulfide bonds), indicating the similar crosslinking efficiency. This result suggests that the partial charge-shielding of PLL segments and ASOs in the core by counter ions (Cl^- and Na^+) probably increased their mobility to facilitate the formation of intermolecular disulfide bonds during PIC/M formation. We further examined the reversible stability of the PIC/Ms after treatment with a reducing agent. A647-ASO-loaded PIC/Ms were prepared at 100 mM NaCl, serially diluted to varying ASO concentrations, and incubated with varying concentrations of gluta-thione (GSH) for 1 h at 37°C, followed by FCS analysis (Figure 2C). The increase in GSH concentration resulted in the decrease in the size of the PIC/M samples, and the decreasing rate was amplified with the decrease in ASO concentration. This result indicated that the PIC/Ms were dissociated under dilute conditions in the presence of GSH, presumably due to the reversible nature of the disulfide crosslinking in the micelle core. Considering that GSH is essential for the cellular detoxification of reactive oxygen species to reduce oxidative stress[18] and its concentration is determined at 0.2–2.7 mM in various brain cells,[19] the PIC/Ms are expected to dissociate after internalization into the cells in the brain parenchyma. Based on these results, the PIC/Ms prepared at 100 mM NaCl were utilized in the following experiments.

Our previous study demonstrated that the glucose ligand density on the nanoparticles was critical for their brain accumulation efficiency, and the optimal ligand density was clearly observed.[7] Accordingly, a series of ASO-loaded PIC/Ms with varying numbers of glucose ligands on their surface were prepared by changing the blending ratio between Glu-PEG-PLL(MPA/IM) (Glu-polymer) and MeO-polymer in the polymer solution. As summarized in Table 1, all Glu-micelles showed similar particle diameters ranging from 42 to 45 nm with PDIs of approximately 0.15, indicating that the glucose ligands barely affected the PIC/M formation (or self-assembling behavior) between the block copolymers and the ASOs. To obtain more detailed structural information, the MWs of the Glu-micelles were determined by analytical

ultracentrifugation (AUC, Table 1).[16,17] Given that PIC/Ms were formed according to the feeding molar ratio (or N/P) of 1.4, the association number of total polymers, namely, Glu-polymer + MeO-polymer, in a single micelle was calculated to be approximately 100 molecules on average. The glucose ligand numbers were then calculated according to the blending ratios between the MeO-polymer and Glu-polymer, which ranged from 0 to 103 (Table 1). Based on these numbers, each PIC/M was abbreviated as Glu(X)-PIC/M, where X represented the number of glucose ligands per particle.

Cellular Uptake of Glu(X)-PIC/Ms in GLUT1-Expressing Cultured Cells

To verify specific molecular interactions of Glu(X)-PIC/Ms with GLUT1, the cellular uptake of Glu(X)-PIC/Ms was evaluated in the cultured human breast cancer cell line MDA-MB-231. This is because MDA-MB-231 cells are known to express high levels of GLUT1 on the surface under culture conditions,[20] which makes them suitable for model GLUT1-expressing cells. A647-ASO-loaded Glu(X)-PIC/Ms (A647-Glu(X)-PIC/Ms) were transfected into the cells and incubated for 1 h at a 400 nM ASO concentration. The fluorescence intensities of A647 were measured with a microplate reader (Supporting Information, Figure S5). The cells treated with the A647-Glu(X)-PIC/Ms with higher glucose numbers showed higher fluorescence intensities, indicating that the A647-Glu(X)-PIC/Ms with higher glucose numbers more efficiently recognized GLUT1 on the cells in the cultured conditions, similar to our previous studies on cancer cells targeted by glucose ligands.[21] Importantly, with the competitive treatment of cells with the GLUT inhibitor phloretin, the fluorescence intensities in the cells treated with A647-Glu-(X)-PIC/Ms were considerably decreased to a similar level as those treated with the control micelle without glucose ligand (A647-Glu(0)-PIC/M). These results demonstrate the enhanced cellular uptake of A647-Glu(X)-PIC/Ms by specific interactions between the glucose ligands and GLUT1. Of note, no saturation of the cellular uptake amount was observed for Glu(100)-PIC/M even at a much higher concentration (for example, 4 μM ASO; data not shown), possibly due to the relatively low binding affinity between glucose and GLUT1.

Table 1: Characteristics of Glu(X)-PIC/Ms with varying numbers of glucose ligands.

Micelle	Blending ratio [Glu:MeO]	Size [nm][a]	PDI[a]	MW [Da]	Association number[b]	Glucose number
Glu(0)	0:100	42±2	0.14±0.03	$1.527×10^6$	96	0
Glu(24)	25:75	42±1	0.16±0.02	$1.567×10^6$	98	24
Glu(52)	50:50	43±2	0.15±0.01	$1.688×10^6$	104	52
Glu(76)	75:25	43±3	0.15±0.01	$1.642×10^6$	101	76
Glu(103)	100:0	45±4	0.15±0.01	$1.679×10^6$	103	103

[a] determined by DLS, [b] determined by AUC.

Blood Circulation and Brain Accumulation of A647-Glu(X)-PIC/Ms

The longevity in blood circulation of Glu(X)-PIC/Ms is more likely to affect the number/probability of contacts between the glucose ligands and GLUT1 molecules on the BCECs, which are critical for crossing the BBB. Thus, the blood circulation properties of A647-Glu(X)-PIC/Ms with varying glucose numbers were examined by in vivo confocal laser scanning microscopy (IVCLSM) in terms of fluorescence intensity of A647 after intravenous injection into the tail veins of mice (Figure 3 A and Supporting Information, Figure S6). While naked A647-ASO exhibited a half-life of 9 min, all A647-Glu(X)-PIC/Ms permitted considerably longer blood retention with half-lives of more than 80 min, regardless of the glucose number. Thus, the installation of glucose ligands was confirmed to induce no considerable alteration of micelle circulation in the bloodstream. Next, the brain accumulation efficiency of A647-Glu(X)-PIC/Ms was evaluated in fasting mice with glycemic control. After fasting the mice for approximately 16 h, a glucose solution (20% w/v in phosphate-buffered saline) was administered intraperitoneally in order to raise the blood glucose level (Supporting Information, Figure S7). At 30 min post-administration of the glucose solution, naked A647-ASO and A647-Glu(X)-PIC/Ms with various glucose numbers were intravenously injected into the tail veins of mice. Notably, a rapid increase in the blood glucose level can trigger the recycling of GLUT1 from the apical to the basal side of the plasma membrane of the BCECs, possibly facilitating the transcytosis of A647-Glu(X)-PIC/Ms.[7] At 1 h post-intravenous administration, the mice were perfused with an excess amount of phosphate-buffered saline and then the whole brain was excised. The brain was homogenized in lysis buffer and fluorescence intensities of A647 in the lysed brain tissues were measured using a microplate reader. Naked A647-ASO and A647-Glu(0)-PIC/M exhibited $0.4 \pm 0.1\%$ and $0.4 \pm 0.3\%$ dose g^{-1} of brain, respectively (Figure 3 B). In contrast, a certain extent of glucose installation onto PIC/Ms (A647-Glu(X)-PIC/Ms: X = 24 and 52) significantly increased their brain accumulation. Notably, A647-Glu(52)-PIC/M achieved the highest brain accumulation efficiency of $6.9 \pm 1.9\%$ dose g^{-1} of brain, which was almost 17-times higher than that of A647-Glu(0)-PIC/M. Interestingly, a further increase in the number of glucose ligands on each of the micelles over 52 led to a steep decrease in the brain accumulation efficiency. Presumably, strong avidity in GLUT1 binding due to an excess glucose density on the A647-Glu(X)-PIC/Ms may have hampered their smooth translocation into the basal side of the BCECs.[7]

The glucose-modified micelle with the highest accumulation efficiency in the whole brain (A647-Glu(52)-PIC/M) was then subjected to further analytical study to evaluate the relative accumulation efficiencies (or accumulation amounts) in different regions of the brain, namely, cerebral cortex, hippocampus, midbrain, thalamus/hypothalamus, and cerebellum. After intravenous injection of A647-Glu(52)-PIC/M into the fasting mice with glycemic control, each brain region was dissected and the fluorescence intensities were measured using a microplate reader. Results are represented as a percentage of the total fluorescence intensity of the whole brain (Figure 3 D). It is worth noting that the highest accumulation amount ($26 \pm 7\%$) was observed in the cerebral cortex. There was an observed amount of approximately 10–17% in the thalamus/hypothalamus, cerebellum, pons, and medulla. The hippocampus, midbrain, and olfactory bulb showed an approximately 7% accumulation amount. The accumulation amounts were further normalized to the weight of each brain area to examine the delivery selectivity of A647-Glu(52)-PIC/M for each brain area (Figure 3 E). Higher normalized values were observed for the thalamus/hypothalamus, cerebellum, olfactory bulb, pons, and medulla compared with the cerebral cortex, hippocampus, and midbrain. This result indicates that Glu(52)-PIC/M has the ability to accumulate in all brain areas with only a moderate tissue selectivity.

MALAT1 Knockdown in Various Brain Regions

The knockdown activity of Glu(X)-PIC/M in the brain was ultimately investigated in the fasting mice with glycemic control. The knockdown efficiencies were determined in both the whole brain and separate brain areas because it is desirable that the ASO drug is delivered to the appropriate area of onset in the diseased brain. For example, the abnormal expansion of CAG repeats in the Huntingtin (*HTT*) gene in HD heavily affects the cortex and striatum.[22] ALS results in dysfunction of motor neurons in the cortex, which induces progressive weakness of muscle.[23] Here, *MALAT1* lncRNA was selected as a model target molecule because *MALAT1* lncRNA is present in a high level in a wide range of mammalian tissues, including brain.[24] The *MALAT1* lncRNA levels were determined by quantitative reverse-transcription PCR (qRT-PCR) and then normalized to that of the housekeeping gene *GAPDH*. *MALAT1*-ASO-loaded Glu(X)-PIC/Ms (100 µg *MALAT1* ASO per injection) were intravenously injected into the tail veins of fasting mice with glycemic control. First, *MALAT1* knockdown efficiency in the whole brain was evaluated at 24 h post-administration (Figure 4 A). Glu(52)-PIC/M exhibited the highest *MALAT1* knockdown efficiency (approximately 30%) among the tested Glu(X)-PIC/Ms. Glu(24)-PIC/M had a modest *MALAT1* knockdown effect (approximately 24%). Glu(24)-PIC/M exhibited a statistical difference with the naked *MALAT1* but not with the other micelle samples. Glu(0)-, Glu(76)-, and Glu(103)-PIC/Ms, as well as naked ASO, exhibited no *MALAT1* knockdown effects. This knockdown efficiency was consistent with the brain accumulation efficiency of the ASO (Figure 3 B).

We further investigated the *MALAT1* knockdown efficiencies of Glu(X)-PIC/Ms in various brain regions, namely, cerebral cortex, hippocampus, midbrain, thalamus/hypothalamus, and cerebellum, at 24 h post-administration (Figure 4 B–F). Glu(X)-PIC/Ms (100 µg *MALAT1* ASO per injection) were intravenously injected into the tail veins of mice under glycemic control. Generally, the *MALAT1* knockdown effect was observed in each region of the brain treated with Glu(24)- and Glu(52)-PIC/Ms, similar to the effect on
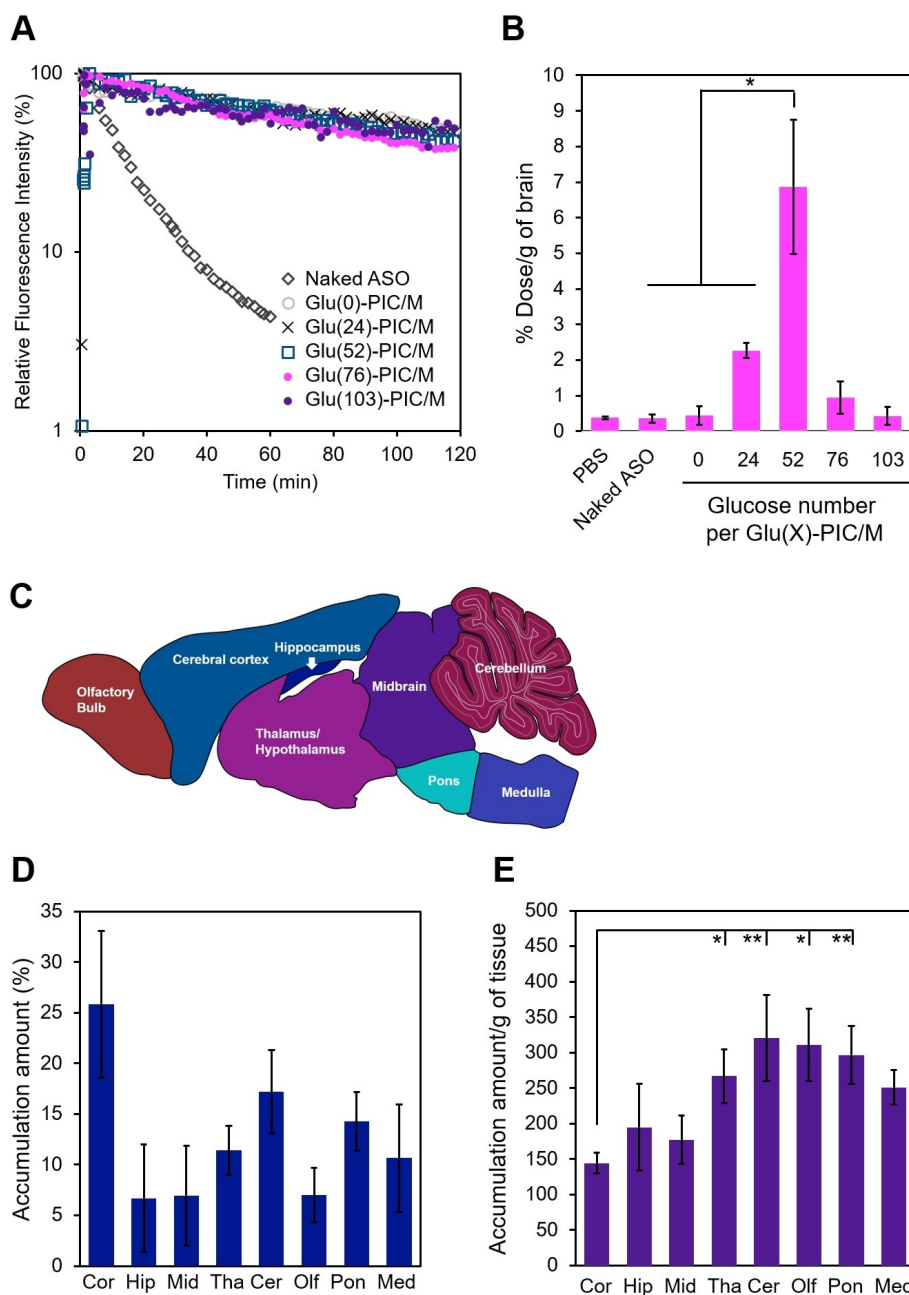
Figure 3. In vivo performances of A647-Glu(X)-PIC/Ms after intravenous administration. A) Blood circulation properties of A647-Glu(X)-PIC/Ms (25 µg A647-ASO) after intravenous administration, determined by IVCLSM. B) Accumulation efficiencies of A647-Glu(X)-PIC/Ms in the whole brain at 1 h post-administration. A647-Glu(X)-PIC/Ms were intravenously administered 30 min after intraperitoneal injection of glucose into fasting mice. The brain was excised and homogenized in the lysis buffer. Fluorescence intensities of lysates were measured using a microplate reader. Results are expressed as mean ± standard deviation ($n = 3$; *$p < 0.05$). C) An illustration of brain sub-regions examined in this study. The brain atlas was slightly modified from a graphical image of gensat.org. D) Fluorescence intensities in various brain regions treated with A647-Glu(52)-PIC/M at 1 h post-injection (25 µg A647-ASO per injection). The fluorescence intensity in each brain region was determined using a microplate reader and normalized to the total fluorescence intensity of all brain regions (Cor: cerebral cortex, Hip: hippocampus, Mid: midbrain, Tha: thalamus/hypothalamus, Cer: cerebellum, Olf: olfactory bulb, Pon: pons, Med: medulla). The micelle sample was administered according to the same injection schedule as in (B). Results are expressed as mean ± standard deviation ($n = 5$). E) Weight-normalized accumulation amounts of A647-Glu(52)-PIC/M in various regions of the brain at 1 h post-administration. Results are expressed as mean ± standard error ($n = 5$; *$p < 0.05$ and **$p < 0.01$).

the whole brain. Notably, Glu(52)-PIC/M exhibited high levels of *MALAT1* knockdown in various regions, such as the cerebral cortex (approximately 54%), hippocampus (approximately 20%), midbrain (approximately 34%), and thalamus/

hypothalamus (approximately 37%), roughly consistent with the apparently uniform distribution of Glu(52)-PIC/M in each brain region (Figure 3E). Interestingly, Glu(52)-PIC/M showed no knockdown effect in the cerebellum even though
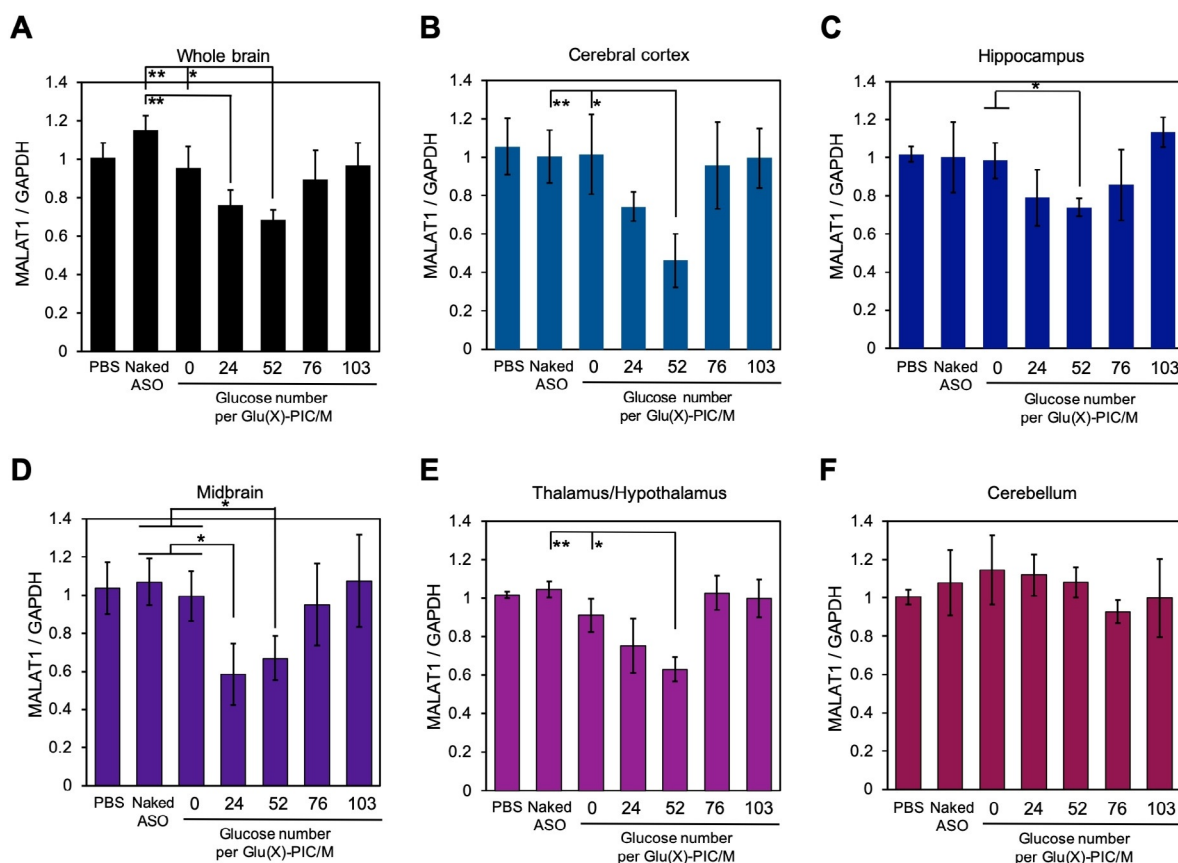
Figure 4. *MALAT1* knockdown efficiencies of Glu(X)-PIC/Ms in the various brain regions in mice 24 h after a single injection (100 μg *MALAT1* ASO). *MALAT1* lncRNA levels were measured in the A) whole brain, B) cerebral cortex, C) hippocampus, D) midbrain, E) thalamus/hypothalamus, and F) cerebellum determined by qRT-PCR. Results are expressed as mean ± standard deviation ($n = 3$; *$p < 0.05$ and **$p < 0.01$).

an appreciable ASO accumulation was observed in this region (Figure 3 E). Glu(24)-PIC/M exhibited less efficient *MALAT1* knockdown, in which only the midbrain (approximately 42%) had a significant difference compared with Glu(52)-PIC/M.

The present delivery strategy for glucose-mediated BBB-crossing can be readily applied for human and nonhuman primates because of the universal expression of GLUT1 on the brain endothelium.[25] The glucose concentration in the fasting mice was approximately 110 mg dL^{-1} and then increased up to 160 mg dL^{-1} after glucose injection.[7] Considering the similar fasting glucose concentration in humans (70–99 mg dL^{-1}), it may be reasonably assumed that the similar glycemic control may trigger the BBB-crossing of glucose-modified nanoparticles. Another issue is repeated administration of Glu(X)-PIC/Ms for ASO therapies, which may result in gradual accumulation of polymer/micelles in the brain. Although we have not studied the clearance of Glu(X)-PIC/Ms from the brain, a recent study reported that meningeal lymphatic vessels in the basal part of the skull are hotspots for the clearance of macromolecules in the cerebrospinal fluid.[26] More detailed clearance mechanism will be investigated in future studies.

Conclusion

We successfully constructed GLUT1-targeted Glu(X)-PIC/Ms and demonstrated the efficient brain accumulation of ASOs by noninvasive intravenous administration. The multiple glucose-modified PIC/Ms dramatically enhanced the brain accumulation efficiency, presumably due to their multivalent binding with GLUT1 expressed on the plasma membrane of the BCECs. GLUT1 at the apical side of the brain vasculature is thought to undergo translocation and recycling triggered by the injection of glucose solution into the fasting mouse. Simultaneously, Glu(X)-PIC/Ms were transferred into the basal side of the BCECs. However, the detailed BBB-crossing mechanism should be further investigated in a future study. The present PIC/Ms are assembled from approximately 100 block copolymer strands and approximately 35 ASO molecules, regardless of glucose numbers, satisfying the following three parameters: i) a size of less than 50 nm, ii) the blood circulation property with half-lives of 80–100 min, and iii) the optimization of glucose number and density (approximately 50 per 100 block copolymer strands) on their surface. Overall, this study provides a unique strategy of noninvasive ASO delivery into the brain using glycemic control as an external trigger, and has an immediate and considerable impact on ASO treatment of CNS disorders

(for example, HD and ALS), symptoms of which mainly occur in the cerebral cortex and hippocampus.

[1] C. Rinaldi, M. J. A. Wood, *Nat. Rev. Neurol.* **2018**, *14*, 9–21.
[2] C. D. Wurster, A. C. Ludolph, *Ther. Adv. Neurol. Disord.* **2018**, *11*, 1–19.
[3] M. M. Evers, L. J. Toonen, W. M. van Roon-Mom, *Adv. Drug Delivery Rev.* **2015**, *87*, 90–103.
[4] C. A. Stein, D. Castanotto, *Mol. Ther.* **2017**, *25*, 1069–1075.
[5] L. Crawford, J. Rosch, D. Putnam, *J. Controlled Release* **2016**, *240*, 251–266.
[6] I. A. Simpson, A. Carruthers, S. J. Vannucci, *J. Cereb. Blood Flow Metab.* **2007**, *27*, 1766–1791.
[7] Y. Anraku, H. Kuwahara, Y. Fukusato, A. Mizoguchi, T. Ishii, K. Nitta, Y. Matsumoto, K. Toh, K. Miyata, S. Uchida, K. Nishina, K. Osada, K. Itaka, N. Nishiyama, H. Mizusawa, T. Yamasoba, T. Yokota, K. Kataoka, *Nat. Commun.* **2017**, *8*, 1001.
[8] S. G. Patching, *Mol. Neurobiol.* **2017**, *54*, 1046–1077.
[9] M. Mammen, S.-K. Choi, G. M. Whitesides, *Angew. Chem. Int. Ed.* **1998**, *37*, 2754–2794; *Angew. Chem.* **1998**, *110*, 2908–2953.
[10] R. J. Christie, Y. Matsumoto, K. Miyata, T. Nomoto, S. Fukushima, K. Osada, J. Halnaut, F. Pittella, H. J. Kim, N. Nishiyama, K. Kataoka, *ACS Nano* **2012**, *6*, 5174–5189.
[11] H. S. Min, H. J. Kim, J. Ahn, M. Naito, K. Hayashi, K. Toh, B. S. Kim, Y. Matsumura, I. C. Kwon, K. Miyata, K. Kataoka, *Biomacromolecules* **2018**, *19*, 2320–2329.
[12] K. Katsushima, A. Natsume, F. Ohta, K. Shinjo, A. Hatanaka, N. Ichimura, S. Sato, S. Takahashi, H. Kimura, Y. Totoki, T. Shibata, M. Naito, H. J. Kim, K. Miyata, K. Kataoka, Y. Kondo, *Nat. Commun.* **2016**, *7*, 13616.
[13] K. Suzuki, Y. Miura, Y. Mochida, T. Miyazaki, K. Toh, Y. Anraku, V. Melo, X. Liu, T. Ishii, O. Nagano, H. Saya, H. Cabral, K. Kataoka, *J. Controlled Release* **2019**, *301*, 28–41.
[14] J. E. G. Barnett, G. D. Holman, K. A. Munday, *Biochem. J.* **1973**, *131*, 211–221.
[15] K. A. Lennox, M. A. Behlke, *Nucleic Acids Res.* **2016**, *44*, 863–877.
[16] K. Hayashi, H. Chaya, S. Fukushima, S. Watanabe, H. Takemoto, K. Osada, N. Nishiyama, K. Miyata, K. Kataoka, *Macromol. Rapid Commun.* **2016**, *37*, 486–493.
[17] H. J. Kim, H. Takemoto, Y. Yi, M. Zheng, Y. Maeda, H. Chaya, K. Hayashi, P. Mi, F. Pittella, R. J. Christie, K. Toh, Y. Matsumoto, N. Nishiyama, K. Miyata, K. Kataoka, *ACS Nano* **2014**, *8*, 8979–8991.
[18] R. Dringen, J. Hirrlinger, *Biol. Chem.* **2003**, *384*, 505–516.
[19] X. Sun, A. Y. Shih, H. C. Johannssen, H. Erb, P. Li, T. H. Murphy, *J. Biol. Chem.* **2006**, *281*, 17420–17431.
[20] M. Grover-McKay, S. A. Walsh, E. A. Seftor, P. A. Thomas, M. J. Hendrix, *Pathol. Oncol. Res.* **1998**, *4*, 115–120.
[21] Y. Yi, H. J. Kim, M. Zheng, P. Mi, M. Naito, B. S. Kim, H. S. Min, K. Hayashi, F. Perche, K. Toh, X. Liu, Y. Mochida, H. Kinoh, H. Cabral, K. Miyata, K. Kataoka, *J. Controlled Release* **2019**, *295*, 268–277.
[22] M. S. Keiser, H. B. Kordasiewicz, J. L. McBride, *Hum. Mol. Genet.* **2016**, *25*, R53–R64.
[23] N. Geevasinga, P. Menon, P. H. Özdinler, M. C. Kiernan, S. Vucic, *Nat. Rev. Neurol.* **2016**, *12*, 651–661.
[24] D. Bernard, K. V. Prasanth, V. Tripathi, S. Colasse, T. Nakamura, Z. Xuan, M. Q. Zhang, F. Sedel, F. Coulpier, A. Triller, D. L. Spector, A. Bessis, *EMBO J.* **2010**, *29*, 3082–3093.
[25] C. C. Barron, P. J. Bilan, T. Tsakiridis, E. Tsiani, *Metabolism* **2016**, *65*, 124–139.
[26] J. H. Ahn, H. Cho, J. H. Kim, S. H. Kim, J. S. Ham, I. Park, S. H. Suh, S. P. Hong, J. H. Song, Y. K. Hong, Y. Jeong, S. H. Park, G. Y. Koh, *Nature* **2019**, *572*, 62–66.